Journal of Electroanalytical Chemistry 855 (2019) 113487

Contents lists available at ScienceDirect

Journal of Electroanalytical Chemistry

journal homepage: www.elsevier.com/locate/jelechem

Ultrasensitive and ultrawide range electrochemical determination of bisphenol A based on PtPd bimetallic nanoparticles and cationic pillar[5]arene decorated graphene

Huan Liang [1], Yuting Zhao [1], Hanzhang Ye, Can-Peng Li [*]

School of Chemical Science and Technology, Yunnan University, Kunming, 650091, PR China

ARTICLE INFO

Keywords:
Electrochemical sensor
Reduced graphene oxide
PtPd bimetallic nanoparticles
Bisphenol A
Pillar[5]arene

ABSTRACT

This study proposed an ultrasensitive and ultrawide range electrochemical sensing platform based on PtPd bimetallic nanoparticles (PtPd NPs) and cationic pillar [5]arene (CP5) decorated graphene for bisphenol A (BPA). CP5-decorated reduced graphene oxide (RGO) (CP5@RGO) was synthesized via a reported assay. PtPd NPs-loaded CP5@RGO nanocomposites (PtPd-CP5@RGO) were then prepared through a simple approach at room temperature. The as prepared materials were characterized by various technologies, including EDX, FT-IR, XRD, TG analysis, XPS, zeta potentiometer, TEM, and AFM. The current response of PtPd-CP5@RGO modified glassy carbon electrode (GCE) to BPA oxidation was higher than that of Pt NPs-, Pd NPs-, or CP5-modified GCE. An electrochemical sensor based on PtPd-CP5@RGO-modified GCE was utilized to determine BPA through differential pulse voltammetry. The sensor yielded the wider linear ranges of 0.01–50 μM and 50–1000 μM, respectively, with a lower limit of detection of 3.3 nM (S/N = 3) for BPA determination. The constructed sensor showed some advantages, such as satisfactory reproducibility, good stability, and excellent selectivity, which was applied to determine BPA concentration in real samples. BPA and CP5 likely formed a stable complex mainly via supramolecular interactions, such as electrostatic and hydrophobic interaction.

1. Introduction

Bisphenol A (BPA) is an important organic compound widely utilized as a monomer to manufacture polymer carbonate plastics, epoxy resins, flame retardants, adhesives, and other substances in polymer industry. BPA is usually found in antibreakage plastics used in metal food containers, the inner surface coating of beverage cans, and food packages [1]. Its toxicity has been widely explored because of its continuous release from beverage cans baby bottles, water bottles, eyeglass lenses, medical devices, and dental products [2–4]. BPA is an endocrine disruptor that can mimic natural hormones, thereby leading to a wide number of diseases, such as obesity, diabetes, thyroid diseases, infertility, hepatic disease, and cancer [5–9]. Currently, many countries (e.g. European Union, China, the United States) have forbidden the use BPA in plastic product and packaging materials [3,4,10]. However, the migration of BPA from wastewater discharge and its leakage to food, drinking water, and environment have shown harmful effects on the health children and infants. Therefore, a simple and rapid assay for BPA determination should be developed.

Various analytical technologies, including HPLC, GC, HPLC–MS, and GC–MS, capillary electrophoresis, fluorescence assay, chemiluminescence detection, and immunoassay assay have been used to determine BPA [11–16]. These methods have demonstrated excellent performances, such as good sensitivity and detection limit, which are favorable for the determination of BPA. However, some disadvantages of these technologies need to be solved analytically, such as costly equipment, time-consuming treatment, strict pretreatments, and skillful technicians, which limit the application of these methods in on-site monitoring or urgent need. Therefore, designing an effective, simple, and fast assay for determination of BPA should be designed.

Pillararenes (PA) is a macrocyclic molecule composed of hydroquinols linked by methylene bridges at parapositions [17]. In the past decade, PA has received much attention, and many functionalized PA derivatives have been successfully synthesized [18,19]. PA shows particular and attractive characteristics, such as convenient synthesis, functionalization, and good solubility in solvents [20]. The symmetry of

* Corresponding author.
E-mail address: lcppp1974@sina.com (C.-P. Li).
[1] These authors contributed equally to this work.

https://doi.org/10.1016/j.jelechem.2019.113487
Received 17 July 2019; Received in revised form 9 September 2019; Accepted 12 September 2019
Available online 13 September 2019

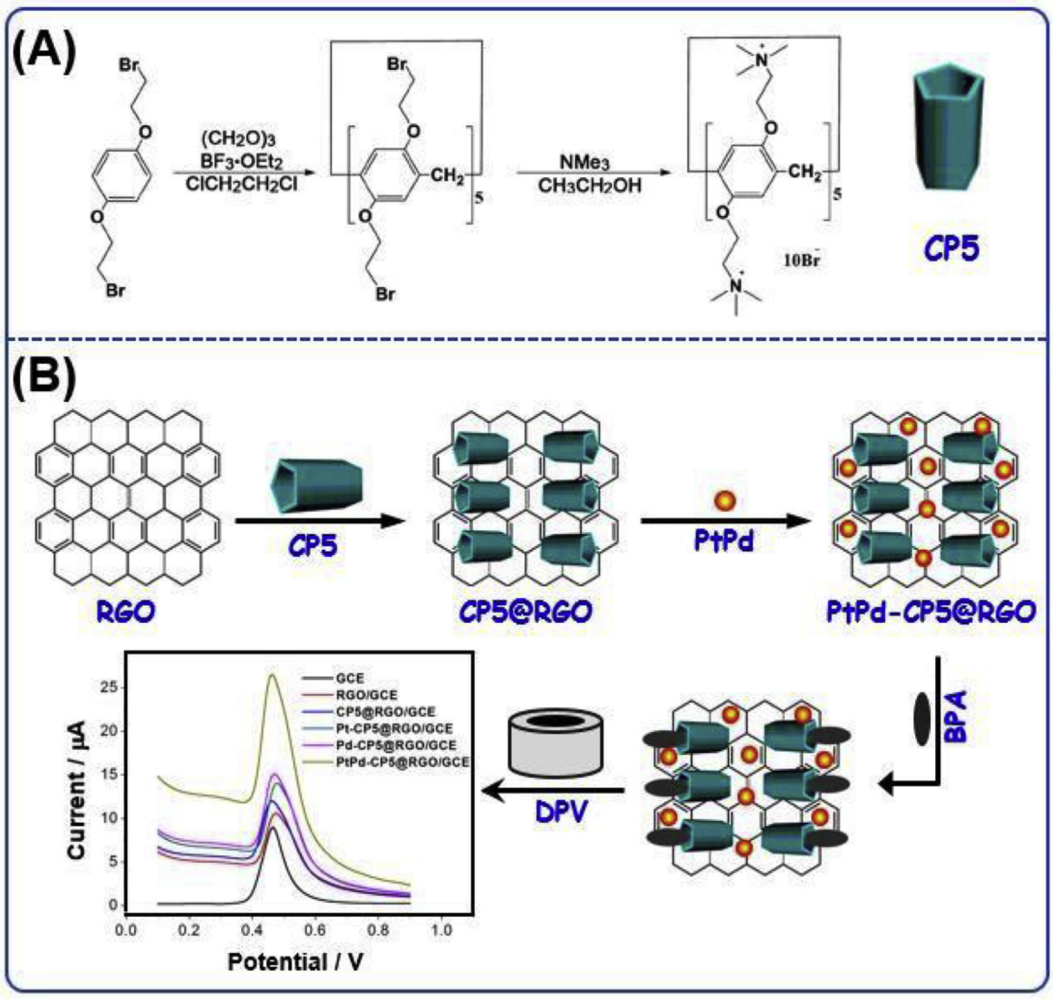

Scheme 1. The synthetic route of CP5 (A) and the illustration of electrochemical sensing strategy for BPA based on PtPd NPs and CP5 decorated graphene (B).

PA is higher and its structures are rigid than those of other macrocyclic molecules. As an electron-rich cavity, PA can excellently recognize various guest molecules [21]. However, studies on the sensors based on PA or PA-functionalized materials are fewer than studies on traditional macrocyclic hosts [22,23].

For electrochemical sensor, the sensitivity can be markedly improved through specific catalyst for signal enhancement. Noble metal nanoparticles (NPs) have caused concerns because of their attractive applications in chemical and biological sensing system [24,25]. Efforts have been devoted to preparing or synthesizing bimetallic nanocomposites with excellent catalytic activity and physiochemical stability compared with those of monometallic NPs [26,27]. Bimetallic NPs are particular important in catalysis because the introduction of the heterogenous metal can result in various shapes, surface morphologies to obtain the desired catalytic activity and chemical selectivity.

Graphene, as a carbon materials with great potential applications in various areas, have been widely explored because of its unmatched structure and properties [28]. Graphene-based materials contain a large amount of oxygen-containing functional groups, which are beneficial to surface modification. Therefore, graphene has been widely used for chemical sensors and biosensors as an outstanding candidate among the available support materials [29].

In the present work, cationic pillar [5]arene (CP5) was prepared (Scheme 1A) and then decorated with reduced graphene oxide (RGO) (CP5@RGO). Then, PtPd NPs-loaded CP5@RGO nanocomposites (PtPd-CP5@RGO) were prepared through a simple approach at room temperature. An electrochemical sensor was fabricated by loading PtPd-CP5@RGO on glassy carbon electrode (GCE) and further successfully employed for BPA determination with good performances, such as wider linear range, lower detection limit, and good stability (Scheme 1B). The excellent electrochemical performance of the sensor for BPA is caused by synergistic influences of RGO, CP5, and PtPd NPs. CP5 can recognize and enrich BPA via host-guest interactions and enhance the concentration of target molecule at the interfaces of PtPd-CP5@RGO modified GCE. RGO is a good electroconductivity material that can efficiently amplify electrical signal of the sensor. PtPd NPs can catalyze the BPA redox reaction, which can amplify the signal of the sensor.

2. Experimental

Experimental details are provided in Supplementary Information.

3. Results and discussion

3.1. Characterization of materials

Fig. 1A shows the FTIR spectra of RGO, CP5, and CP5@RGO. Several stretching vibrations, such as 1612 cm^{-1} (carbon-carbon double bond), 1090 cm^{-1} (carbon-carbon/carbon oxygen bonds), and 3428 cm^{-1}(hydroxy), were clearly found in RGO, indicating the presence of the remanent O-containing groups. The wavenumber at 3350 cm^{-1} belonged to carbon oxygen stretching vibrations, which could be from CP5 in

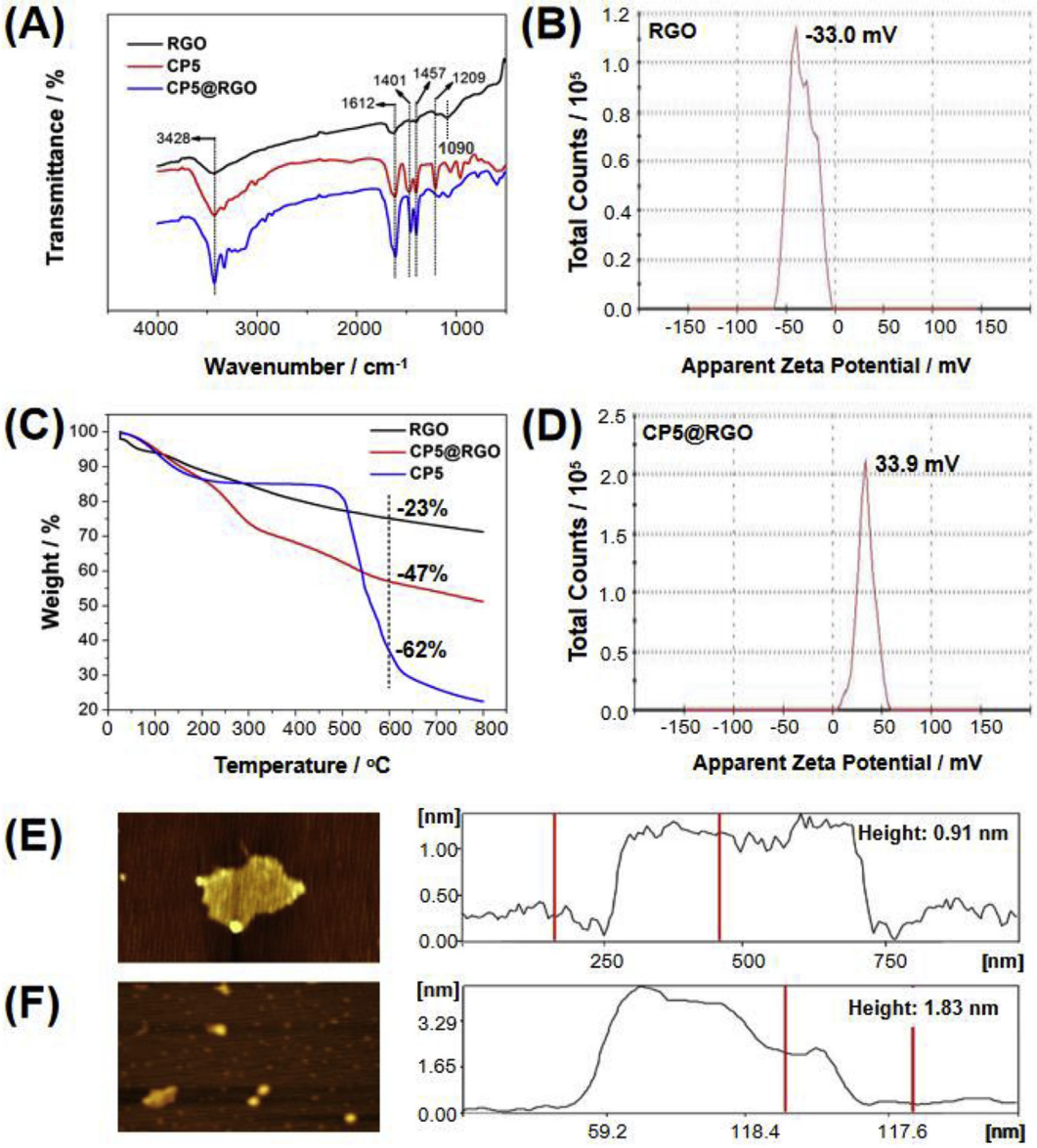

Fig. 1. Characterization of materials. FTIR spectra of RGO, CP5, and CP5@RGO (A); Zeta potentials of RGO and CP5@RGO (**B, D**); TGA curves of RGO, CP5, and CP5@RGO (**C**); AFM images of RGO (**E**) and CP5@RGO (**F**).

CP5@RGO. The bands at 1612, 1457, 1401 and 1209 cm^{-1} corresponded to the stretching vibrations of benzene skeleton, suggesting that CP5 was successfully integrated in RGO. This result was consistent with that of cationic pillar [6]arene-modified RGO in our recent work [23]. Thermogravimetric analysis (TGA) was performed to gain the loaded amount of CP5 in CP5@RGO nanocomposite. In Fig. 1C, RGO displayed a mass loss of 23% at 600 °C due to the mass loss is caused by degradation of the organic O-containing functional groups in RGO [23]. CP5@RGO showed a sudden mass loss when the temperature reached 500 °C because of the pyrolysis of CP5 (Fig. 1C). Here, the mass showed a loss of ~ 47% at 600 °C. Therefore, the mass loss of the bound CP5 with RGO is calculated approximately at 15% by subtracting of RGO from that of CP5@RGO. The result indicates that supramolecular host CP5 was successfully loaded to RGO. The ζ-potential measurements of materials were obtained. The ζ-potential of RGO and CP5@RGO were −33.0 and 33.9 mV, respectively (Fig. 1B, D), which were attributed to the introduced positive charges of CP5 molecule. This result indicated that CP5 was effectively introduced to CP5@RGO and form a stable nanocomposite. The atomic force microscope (AFM) images of the materials were obtained. In Fig. 1E and F, thickness of the RGO is 0.91 nm, whereas the thickness of CP5@RGO increases to 1.83 nm. This result indicated that increased thickness of CP5@RGO was due to the loaded CP5 on the RGO surface.

Energy dispersive X-ray spectroscopy was conducted to explore elements of nanocomposite. C, N, O, Pd, and Pt elements were confirmed in CP5@RGO indicating that the CP5 and PtPd NPs were successfully loaded to RGO. The crystal structures of PtPd-CP5@RGO were investigated through XRD. In Fig. 2B, a peak appeared at 26° (2θ) in PtPd-CP5@RGO, which is the diffraction peak of the RGO. Four diffraction peaks were found at 40.6°, 47.1°, 69.2°, and 83.4° (2θ) attributed to Pt(111)/Pd(111), Pt(200)/Pd(200), Pt(220)/Pd(220), and Pt(311)/Pd(311), respectively [30], indicating that PtPd NPs were successfully prepared. XPS was performed to investigate the nature of the C, N, O, and metal species in PtPd-CP5@RGO.PtPd-CP5@RGO was mainly composed of C, N, O, Pd, and Pt elements (Fig. 2C), and this finding was consistent with that of EDX. In the C1s spectrum, the peaks observed at 284.74, 285.59, 286.67, 287.65, and 288.83 eV corresponded to C═C, C–C, C–O, C═O, and O–C═O bonds, respectively. However, the intensities of peaks of C═C/C–C in PtPd-CP5@RGO became dominant, and the intensities of

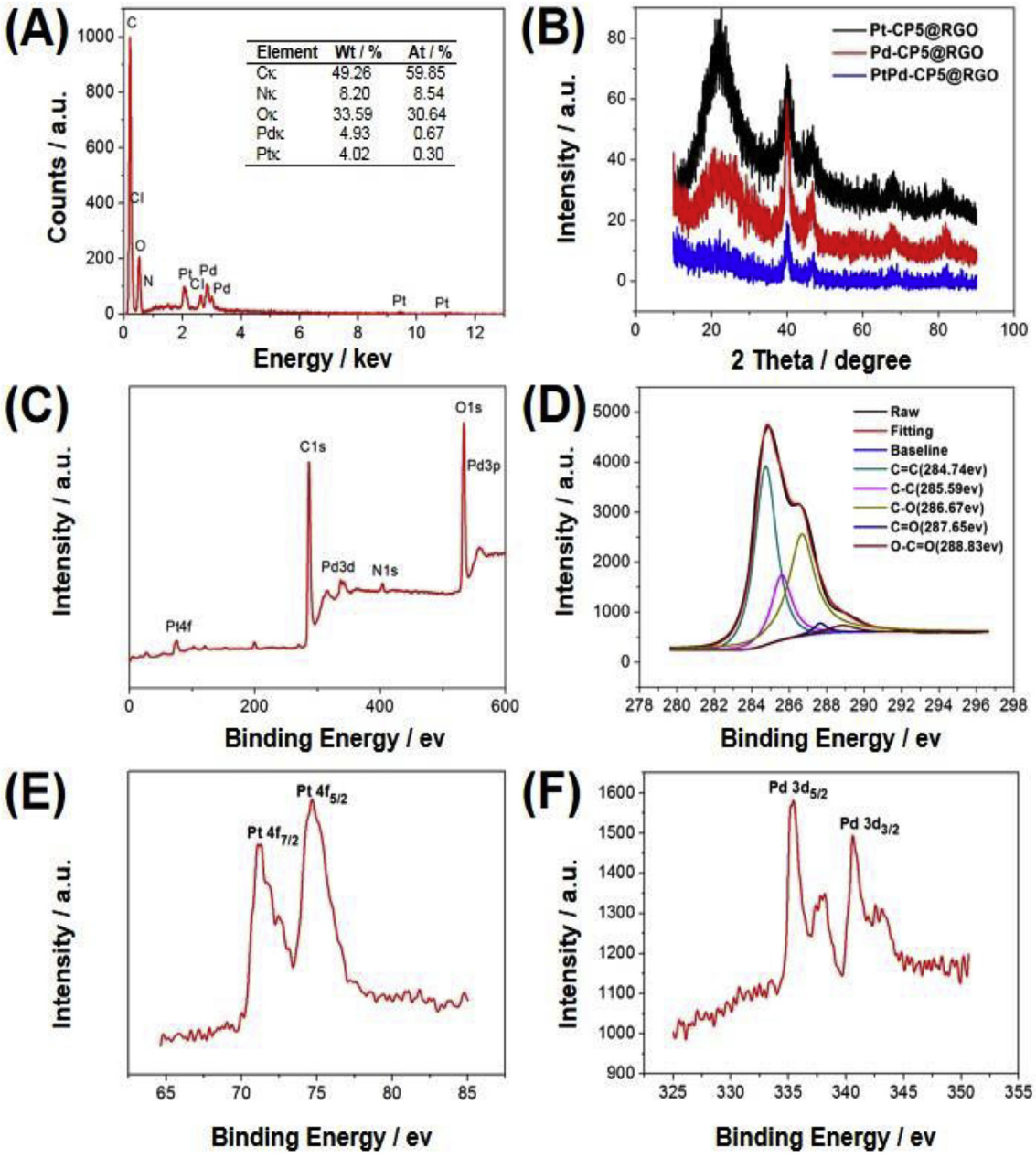

Fig. 2. Characterization of PtPd-CP5@RGO. EDX (A); XRD (**B**); XPS survey spectrum (**C**); the narrow spectra of C 1s, Pt 4f, and Pd 3d (**D, E, F**).

C1s peaks of C bound to O (C═O, C–O, and O–C–O) decreased markedly comparing with that of GO [22]. This result further demonstrated that O-containing groups in RGO was removed after the reduction reaction. The appearance of peaks at 71 and 74 eV could be ascribed to Pt $4f_{7/2}$ and Pt $4f_{5/2}$, and the characteristic peaks at 335.1 and 340.5 eV are assigned to Pd $3d_{5/2}$ and Pd $3d_{3/2}$, respectively [31]. The morphological characteristics of PtPd-CP5@RGO was observed in the TEM image. In Fig. 3A–C, PtPd NPs were well dispersed on RGO's surface with diameters ranging from 10 nm to 20 nm. Fig. 3D shows the scanning TEM image of PtPd NPs selected in Fig. 3C. The image clearly shows the simultaneous distribution of C, N, O, Pd, and Pt elements. All these results demonstrated that PtPd-CP5@RGO was successfully prepared.

3.2. Electrochemical response of BPA

The electrochemical response of BPA at various electrodes were tested by CV and DPV. For better comparison of modified electrodes and to see the redox process, the CVs responses of various materials-modified electrodes towards BPA were studied (Fig. S3). The CV of the resulting electrode displayed an oxidation peak at around 0.55 V. The potential of the electrode slightly positive-shifted and increased significantly after loading with RGO, CP5@RGO, Pt-CP5@RGO, or Pd-CP5@RGO, PtPd-CP5@RGO, suggesting that these materials catalysed the electrochemical oxidation of BPA. Meanwhile, the potential shift also may be due to the supramolecular interactions between CP5 and BPA. It is worthy to note that, PtPd-CP5@RGO nanocomposite had the highest response towards BPA among these materials, indicated that it could be used as a signal amplifier. Furthermore, DPVs of the material modified GCE were investigated. In Fig. 4A, DPV of the GCE displays a current peak of 12.2 μA at 0.55 V in the presence of 1.0 mM of BPA at pH 6.0 (0.1 M PBS), and this observation belonged to oxidation of hydroxy group of the BPA molecule. The current of BPA slightly increased at the RGO modified GCE because of the good conductivity, specific surface area, and electrocatalytic activity of RGO. The current of BPA further increased at the CP5-, Pt NPs-,

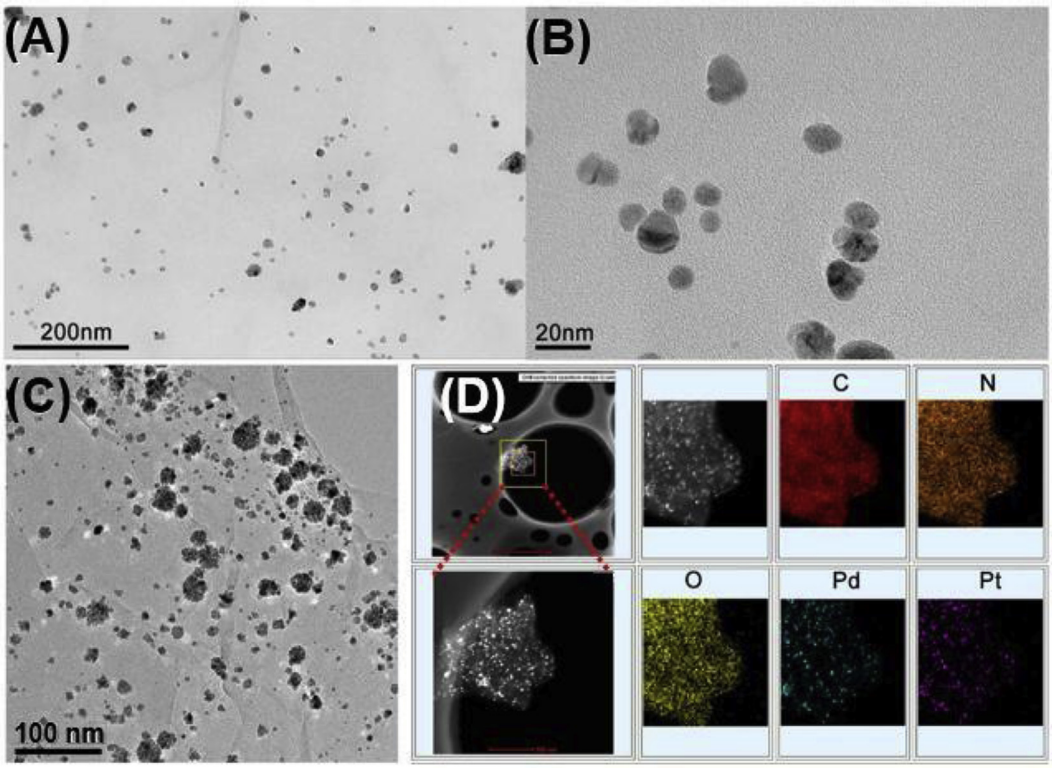

Fig. 3. TEM images of PtPd-CP5@RGO at different magnifications (A, B, C); Elements mapping (C, N, O, Pd, and Pt) of PtPd-CP5@RGO (**D**).

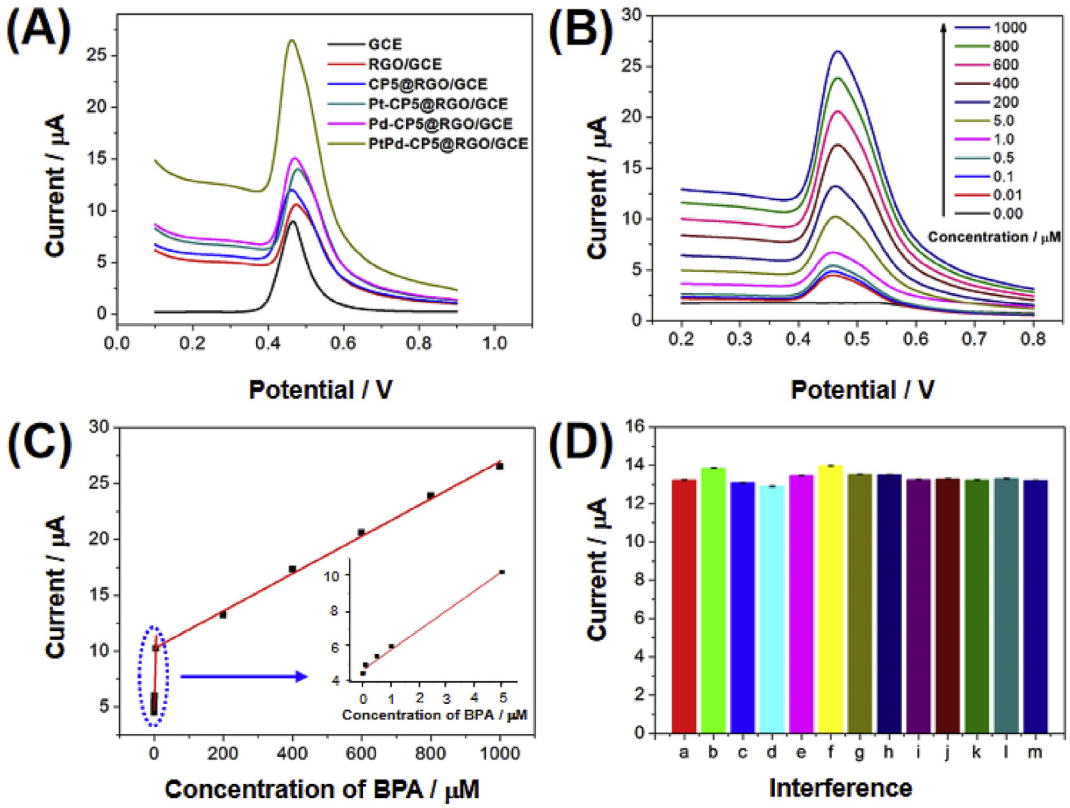

Fig. 4. DPV of 1.0 mM BPA at bare GCE, RGO/GCE, CP5@RGO/GCE, Pt-CP5@RGO/GCE, Pd-CP5@RGO/GCE, and PtPd-CP5@RGO/GCE in 0.1 M PBS solution (pH 6.0). Pulse width: 0.05 s; amplitude: 0.05 V (A). DPV curves for the oxidation of BPA concentrations at PtPd-CP5@RGO/GCE (B) in 0.1 M PBS solution (pH 6.0). Calibration curves for determination of BPA using the proposed sensor (C). The response currents of 100 μM BPA at the proposed sensor recorded in the presence of various interferences. a, 100 μM BPA; b-h, 100 μM BPA in the presence of 100 mM of *o*-aminophenol, *p*-aminophenol, *m*-aminophenol, phenol, *o*-catechol, p-catechol, or *m*-catechol; i-m, 100 μM BPA in the presence of 100 mM of Cl^-, Hg^{2+}, Fe^{3+}, Zn^{2+}, or SO_4^{2-} (D).

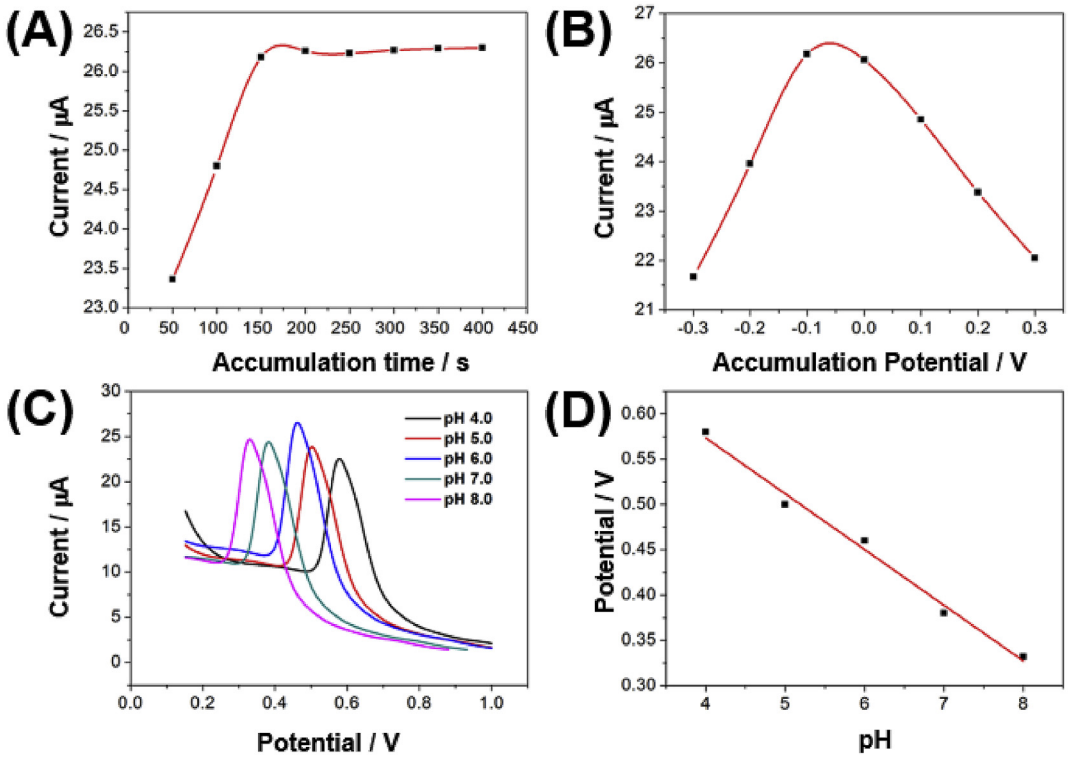

Fig. 5. Effect of accumulation time **(A),** accumulation potential **(B),** and pH (**C**) on the oxidation peak current of 1.0 mM BPA at PtPd-CP5@RGO/GCE in 0.1 M PBS (pH 6.0) by DPV. Pulse width: 0.05 s; amplitude: 0.05 V. Variations of the peak potentials *vs* pH of the detection medium (**D**).

or Pd NPs-modified RGO because of the enrichment/recognition of BPA by CP5 or the catalytic effect of monometallic NPs (Pt NPs or Pd NPs). However, the PtPd-CP5@RGO modified GCE exhibited the highest oxidation current of BPA among the GCEs. The enhanced electrochemical behavior was attributed to the synergistic effect of high-efficiency catalytic activity of PtPd @RGO and the excellent BPA enrichment by CP5 molecule. These results supported the feasibility by using PtPd NPs and CP5 as highly amplifying materials to construct novel electrochemical sensor for BPA.

3.3. Optimization of experimental conditions

The accumulation time and potential of PtPd-CP5@RGO/GCE to BPA were optimized because the accumulation process is an effective strategy to improve sensitivity. The oxidation current increases as the accumulation time was extended from 50 s to 150 s, but the current became stable after 200 s (Fig. 5A). This result suggested that the accumulation of BPA on the PtPd-CP5@RGO/GCE could reach a state of saturation. The peak current of BPA increased as the accumulation potential increased, but this current markedly decreased at −0.1 V (Fig. 5B). Thus, 200 s and −0.1 V were used as the optimal accumulation conditions in this study. The current response of BPA at the surface of PtPd-CP5@RGO/GCE was investigated ranging the pH 4.0–8.0 because pH can influence the rate of mass transport to the electrode. In Fig. 5C, the peak currents of BPA gradually increased when pH increased from 4.0 to 6.0, and the current decreased at pH from 6.0 to 8.0. Therefore, pH 6.0 was selected as the optimized parameter for BPA measurement. Here, the optimum pH (6.0) of BPA was smaller than its pKa, indicating that undissociated BPA may be adsorbed on PtPd-CP5@RGO/GCE to a great extent than the dissociated one [32]. In the present work, BPA could enter the cavity of CP5 and form a steady inclusion through hydrophobic and electrostatic interactions, which were discussed below and in the later section of Molecule docking. The peak potential of BPA was tested in media with various pH to investigate the electron transfer of BPA at the PtPd-CP5@RGO/GCE. In Fig. 5D, linear relation can be observed between the potentials of BPA and pH with the following regression equation: Ep (V) = −0.0616 pH + 0.8201. The shifted potential (slope) of BPA is 61.6 mV/pH unit, which is almost equal to the theoretical value (59 mV/pH unit), suggesting that the electrons are transferred via an equal number of protons at the surface of the modified electrode [32]. The CVs of BPA at PtPd-CP5@RGO/GCE with various scan rates were obtained to determine the oxidation mechanism. The oxidation current increased ranging from 34.3 to 128.9 μA as the scan rate increased equation of Epa (V) = 0.03007 lnv + 0.551 (r^2 = 0.9952) (Fig. 6C) in accordace with the Laviron equation [33]. The results suggests that oxidation of BPA on PtPd-CP5@RGO/GCE surface is a representative adsorption-controlled process, further confirming that PtPd-CP5@RGO is an excellent nanocomposite for electrochemical BPA determination.

3.4. Electrochemical behavior of BPA

Under the optimal analytical conditions, DPV was recorded and used to determine BPA. The peak current increased as the BPA concentration increased (Fig. 4B). The currents were proportional to the BPA concentrations ranging from 0.01 to 50 μM and 50–1000 μM, respectively, with a detection limit of 3.3 nM (S/N = 3). The corresponding regression equations were calculated as I (μA) = 1.107C (μM) + 4.730 and I (μA) = 0.01672C (μM) + 10.246 with correlation coefficients of 0.996 and 0.994, respectively (Fig. 4C). The detection performance of constructed sensor was compared with that of previously reported ones (Table 1). The detection of limit of the PtPd-CP5@RGO/GCE based sensor was lower and its wide linear range was wider than those of previously reported ones [34–44], possibly because of the outstanding electrocatalytic property of PtPd NPs-loaded RGO and the pre-eminent adsorption capacity of CP5. Since HPLC is a classical method for BPA determination, the comparation of BPA quantitative analysis in real samples were performed by HPLC and the proposed electrochemical sensor. Both methods show the satisfactory results for BPA determination in real samples (Table S1).

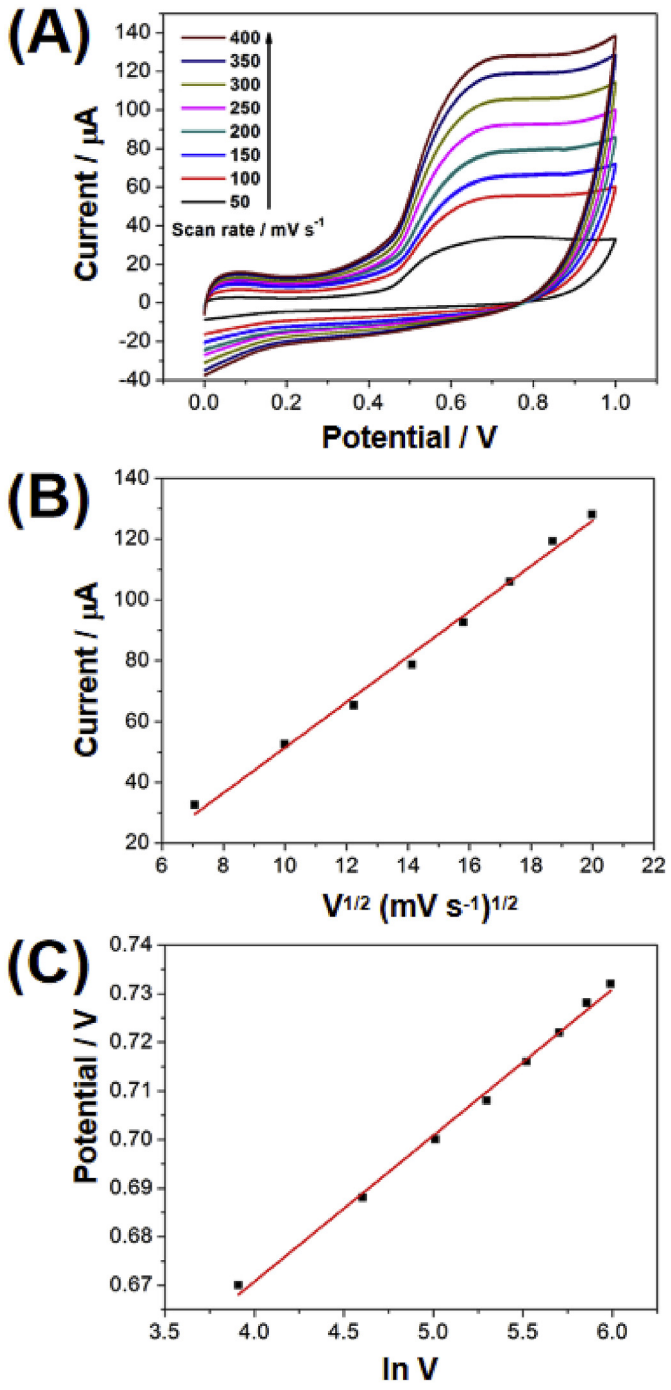

Fig. 6. CVs obtained of the oxidation of 1.0 mM BPA at PtPd-CP5@RGO/GCE in 0.1 M PBS (pH 6.0) at various scan rates ranging 50–400 mV s^{-1}; Magnitude of oxidation peak current *vs.* square root of scan rate (**A**); Variations of the oxidation peak current *vs* the square root of the scan rates (**B**); Variations of the oxidation peak potential *vs* the natural log of the scan rates (**C**).

3.5. Selectivity, reproducibility, and stability of the constructed sensor

Some potential interferences, such as phenolics and inorganic salt were performed using the proposed sensor in the detection. The oxidation currents of 100 μM BPA on the PtPd-CP5@RGO/GCE were compared with those of current signals in the presence interfering species. Fig. 4D shows that the presence of the interferences (10-fold concentration of the target) did not affect the current response of the sensor, indicating good selectivity. The reproducibility of the sensors was evaluated on six PtPd-CP5@RGO/GCEs by using the oxidation peak currents of 100 μM BPA. The oxidation currents of the modified electrodes were approximately similar to the relative the standard deviation (RSD) of 3.21% and 4.68% by using the same sensor and different sensors, respectively (Table S2). This finding indicated satisfactory reproducibility and repeatability. For the stability evaluation of the sensor, six electrodes were prepared independently. After stored at 4 °C for 0–4 weeks, the peak currents response of the electrodes remain 94.80%–99.42% of the initial value (Table S3), indicating a good stability of the proposed sensor.

Table 1
Comparison of the constructed electrochemical sensor for BPA detection with others.

Electrode	Method	Liner range (μM)	Detection limit (nM)	Ref.
CTAB/Ce-MOF/GCE	DPV	0.005–50	2	[32]
ITO	DPV	5–120	290	[35]
CS-Fe_3O_4/GCE	DPV	0.05–30.0	8	[36]
Pd@TiO_2–SiC/GCE	DPV	0.01–5, 5–200	4.3	[37]
MIPPy/GQDs/GCE	DPV	0.1–50	40	[38]
MWCNTs/GCE	DPV	4.9–82.5	84	[39]
MWCNTs-PEI/GCE	DPV	0.01–50	3.3	[40]
MPL-NiS/rGO/GCE	ASV	0.0005–0.053	0.4	[41]
DPNs/GCE	Amp	0.01–1.0, 1.0–300	6.6	[42]
MWCNT-Au NPs/GCE	Amp	0.01–0.7	4.3	[43]
MWCNT-PDDA-AuPd/GCE	DPV	0.18–18	60	[44]
CoPc-CPE	DPV	0.088–12.5	10	[45]
PtPd-CP5@RGO/GCE	DPV	0.01–50, 50–1000	3.3	This work

Table 2
Determination of BPA in water and milk samples by proposed sensor (n = 4).

Sample	Added (μM)	Founded (μM)	RSD (%)	Recovery (%)
Tap water	4.0	3.91 ± 0.09	3.2	97.75
	8.0	8.13 ± 0.11	4.1	101.63
	50.0	49.08 ± 1.69	3.8	98.16
Lake water	4.0	4.09 ± 0.13	3.7	102.25
	8.0	8.07 ± 0.21	2.8	100.88
	50.0	52.35 ± 2.27	4.6	104.70
Milk	1.0	0.96 ± 0.03	3.5	96.00
	5.0	5.08 ± 0.09	2.4	101.60
	20.0	19.17 ± 0.36	4.3	95.85

3.6. Measurement of BPA in real samples

The standard addition method was utilized to measure BPA concentration in water samples and to evaluate feasibility of the constructed sensor for the practical BPA determination. The recoveries of BPA in tap water and lake water in the ranged from 97.75% to 104.70% (Table 2), suggesting that the proposed sensor had satisfactory accuracy and could meet the demand for BPA determination in true samples.

3.7. Molecular docking

Molecular docking was performed to explore the interactions between host and guest. Binding mode of BPA with CP5 was simulated by DOCK6.7 program. The docking scores of CP5/BPA complex were obtained (Table S4). The energy scores of conformation of CP5/BPA complex was −27.86 kcal mol^{-1}. In Table S5, the ΔGbind of the CP5/BPA complex calculated by MM-GBSA method (ΔGbind = ΔGvdw +ΔGes + ΔGpol + ΔGapol) were −18.54 kcal mol^{-1}. In Fig. 7, the BPA molecule was included into the upper part of CP5's cavity through a Γ-type binding. Meanwhile, one of the phenolic hydroxyls of BPA was located at the center of cavity and surrounded by positively charged trimethylamine groups, forming Γ-type and parallel accumulation interaction with

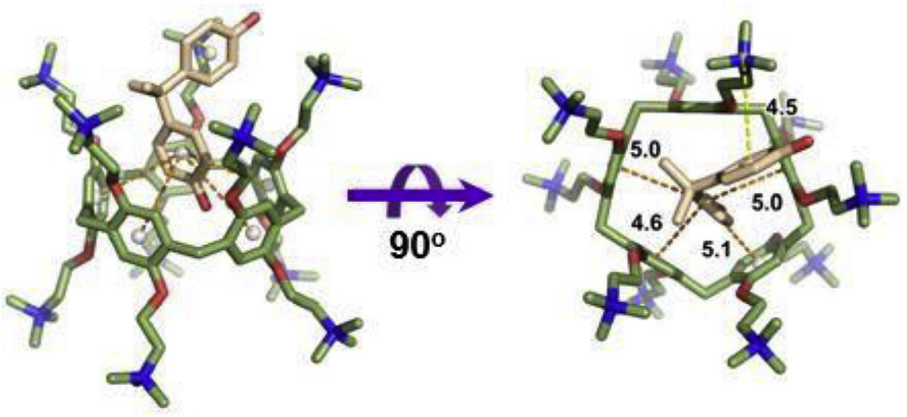

Fig. 7. Conformation of the CP5/BPA complex by molecular docking.

benzene rings. Secondly, cationic bond was formed between the trimethylamine groups and another phenolic hydroxyls of the BPA with bond length of 4.6–5.1 Å. Therefore, the electrostatic force contribution from the hydrogen bonding and π interaction was obtained as $-15.89\ \text{kcal mol}^{-1}$. The corresponding van der Waals contribution was $-26.34\ \text{kcal mol}^{-1}$. Thirdly, hydrophobic interactions between the benzene of BPA and the hydrophobic cavity of CP5 could be observed and played an important role in stabilization of host-guest complex. All of the above interactions are considered playing key roles in stabilizing the host−guest complex.

4. Conclusion

In summary, we developed an electrochemical determination of BPA based on PtPd NPs and CP5 decorated RGO. Under the optimal experimental conditions, the constructed sensor exhibits low detection limit, wide range, better anti−interference, good stability, and satisfactory repeatability. The excellent performance could be attributed to the synergistic effects of electrocanalytic property by RGO, PtPd NPs, and the preeminent adsorption capacity of CP5. Furthermore, the prepared sensor exhibits better electrochemical parameters than those reported previously. The sensor was utilized to measure BPA in true water sample with satisfactory recoveries. Moreover, BPA may be included by CP5 and form a stable inclusion by molecular docking.

Conflicts of interest

There are no conflicts to declare.

Acknowledgements

This work was financially supported by the National Natural Science Foundation of China (21764005, 21565029), Key Projects of Yunnan Natural Science Foundation (2018FA005), Key Research and Development Projects of Yunnan (2018BC005), Program for Excellent Young Talents of Yunnan University, and the Program for Donglu Scholars of Yunnan University.

Appendix A. Supplementary data

Supplementary data to this article can be found online at https://doi.org/10.1016/j.jelechem.2019.113487.

References

[1] X.L. Cao, J. Corriveau, Survey of bisphenol A in bottled water products in Canada, Food Addit. Contam. B 1 (2008) 161–164.
[2] A.V. Krishnan, P. Stathis, S.F. Permuth, L. Tokes, D. Feldman, Bisphenol-A: an estrogenic substance is released from polycarbonate flasks during autoclaving, J. Endocrinol. 132 (1993) 2279–2286.
[3] Y. Gao, Y. Cao, D. Yang, X. Luo, Y. Tang, H. Li, Sensitivity and selectivity determination of bisphenol A using SWCNT-CD conjugate modified glassy carbon electrode, J. Hazard Mater. 199 (2012) 111–118.
[4] L. Wu, D. Deng, J. Jin, X. Lu, J. Chen, Nanographene-based tyrosinase biosensor for rapid detection of bisphenol A, Biosens. Bioelectron. 35 (2012) 193–199.
[5] R.S. Strakovsky, H. Wang, N.J. Engeseth, J.A. Flaws, W.G. Helferich, Y.X. Pan, S. Lezmi, Developmental bisphenol A (BPA) exposure leads to sex-specific modification of hepatic gene expression and epigenome at birth that may exacerbate high-fat diet-induced hepatic steatosis, Toxicol. Appl. Pharmacol. 284 (2015) 101–112.
[6] T. Pollock, D. deCatanzaro, Presence and bioavailability of bisphenol A in the uterus of rats and mice following single and repeated dietary administration at low doses, Reprod. Toxicol. 49 (2014) 145–154.
[7] B.M. Angle, R.P. Do, D. Ponzi, R.W. Stahlhut, B.E. Drury, S.C. Nagel, W.V. Welshons, C.L. Besch−Williford, P. Palanza, S. Parmigiani, F.S. vom Saal, J.A. Taylor, Metabolic disruption in male mice due to fetal exposure to low but not high doses of bisphenol A (BPA): evidence for effects on body weight, food intake, adipocytes, leptin, adiponectin, insulin and glucose regulation, Reprod. Toxicol. 42 (2013) 256–268.
[8] P. Wisniewski, R.M. Romano, M.M. Kizys, K.C. Oliveira, T. Kasamatsu, G. Giannocco, M.I. Chiamolera, M.R. Dias-da-Silva, M.A. Romano, Adult exposure to bisphenol A (BPA) in Wistar rats reduces sperm quality with disruption of the hypothalamic-pituitary-testicular axis, Toxicol. Sci. 329 (2015) 1–9.
[9] M.S. Rahman, W.S. Kwon, J.S. Lee, S.J. Yoon, B.Y. Ryu, M.G. Pang, Bisphenol-A affects male fertility via fertility-related proteins in spermatozoa, Sci. Rep. 5 (2015) 1–9.
[10] M.S. Cosio, A. Pellicanò, B. Brunetti, C.A. Fuenmayor, A simple hydroxylated multi-walled carbon nanotubes modified glassy carbon electrode for rapid amperometric detection of bisphenol A, Sens. Actuators B Chem. 246 (2017) 673–679.
[11] J. Sajiki, K. Takahashi, J. Yonekubo, Sensitive method for the determination of bisphenol-A in serum using two systems of high-performance liquid chromatography, J. Chromatogr. B 736 (1999) 255–261.
[12] S.M. Zimmers, E.P. Browne, P.W. O'Keefe, D.L. Anderton, L. Kramer, D.A. Reckhow, K.F. Arcaro, Determination of free Bisphenol A (BPA) concentrations in breast milk of U.S. women using a sensitive LC/MS/MS method, Chemosphere 104 (2014) 237–243.
[13] S. Alsudir, Z. Iqbal, E.P.C. Lai, Competitive CE-UV binding tests for selective recognition of bisphenol A by molecularly imprinted polymer particles, Electrophoresis 33 (2012) 1255–1262.
[14] Y. Zhu, Y. Cai, L. Xu, L. Zheng, L. Wang, B. Qi, C. Xu, Building an aptamer/graphene oxide FRET biosensor for one-step detection of bisphenol A, ACS Appl. Mater. Interfaces 7 (2015) 7492–7496.
[15] E. Maiolini, E. Ferri, A.L. Pitasi, A. Montoya, M.D. Giovanni, E. Errani, S. Girotti, Bisphenol A determination in baby bottles by chemiluminescence enzyme-linked immunosorbent assay, lateral flow immunoassay and liquid chromatography tandem mass spectrometry, Analyst 139 (2014) 318–324.
[16] M.P. Zhao, Y.Z. Li, Z.Q. Guo, X.X. Zhang, W.B. Chang, A new competitive enzyme-linked immunosorbent assay (ELISA) for determination of estrogenic bisphenols, Talanta 57 (2002) 1205–1210.
[17] T. Ogoshi, S. Kanai, S. Fujinami, T.A. Yamagishi, Y. Nakamoto, para-Bridged symmetrical pillar [5] arenes: their Lewis acid catalyzed synthesis and host–guest property, J. Am. Chem. Soc. 130 (2008) 5022–5023.
[18] M. Cao, Y. Hao, Z. Xu, S.H. Liu, J. Yin, The synthetic chemistry of pillar[n]arenes, Curr. Org. Chem. 20 (2016) 1299–1313.
[19] M. Xue, Y. Yang, X. Chi, Z. Zhang, F. Huang, Pillararenes, a new class of macrocycles for supramolecular chemistry, Acc. Chem. Res. 45 (2012) 1294–1308.
[20] Z.Y. Li, Y. Zhang, C.W. Zhang, L.J. Chen, C. Wang, H.W. Tan, Y.H. Yu, X.P. Li, H.B. Yang, Cross-linked supramolecular polymer gels constructed from discrete

multi-pillar[5]arene metallacycles and their multiple stimuli-responsive behavior, J. Chem. Soc. 136 (2014) 8577–8589.
[21] J.F. Sun, B. Hua, Q. Li, J. Zhou, J. Yang, Acid/base-controllable FRET and self-assembling systems fabricated by rhodamine B functionalized pillar[5]arene-based host-guest recognition motifs, Org. Lett. 20 (2018) 365–368.
[22] G.F. Zhao, L. Yang, S.L. Wu, H. Zhao, E. Tang, C.P. Li, The synthesis of amphiphilic pillar[5]arene functionalized reduced graphene oxide and its application as novel fluorescence sensing platform for the determination of acetaminophen, Biosens. Bioelectron. 91 (2017) 863–869.
[23] S. Tan, R. Han, S.L. Wu, H. Liang, Y.T. Zhao, H. Zhao, C.P. Li, A novel fluorescent sensing platform for insulin detection based on competitive recognition of cationic pillar[6]arene, Talanta 197 (2019) 130–137.
[24] T.K. Sau, A.L. Rogach, F. Jäckel, T.A. Klar, J. Feldmann, Properties and applications of colloidal nonspherical noble metal nanoparticles, Adv. Mater. 22 (2010) 1805–1825.
[25] K. Saha, S.S. Agasti, C. Kim, X. Li, V.M. Rotello, Gold nanoparticles in chemical and biological sensing, Chem. Rev. 112 (2012) 2739–2779.
[26] Y. Xia, Y. Xiong, B. Lim, S.E. Skrabalak, Shape-controlled synthesis of metal nanocrystals: simple chemistry meets complex physics? Angew. Chem. Int. Ed. 48 (2009) 60–103.
[27] L. Wang, Y. Nemoto, Y. Yamauchi, Direct synthesis of spatially-controlled Pt-on-Pd bimetallic nanodendrites with superior electrocatalytic activity, J. Am. Chem. Soc. 133 (2011) 9674–9677.
[28] M.J. Allen, V.C. Tung, R.B. Kaner, Honeycomb carbon: a review of graphene, Chem. Rev. 110 (2010) 132–145.
[29] S. Taniselass, M.K.M. Arshad, S.C.B. Gopinath, Graphene-based electrochemical biosensors for monitoring noncommunicable disease biomarkers, Biosens. Bioelectron. 130 (2019) 276–292.
[30] C.H. Wang, C.H. Yang, J.K. Chang, High-selectivity electrochemical non-enzymatic sensors based on graphene/Pd nanocomposites functionalized with designated ionic liquids, Biosens. Bioelectron. 89 (2017) 483–488.
[31] R. Zhang, C.L. Sun, Y.J. Lu, W. Chen, Graphene nanoribbon-supported PtPd concave nanocubes for electrochemical detection of TNT with high sensitivity and selectivity, Anal. Chem. 87 (2015) 12262–12269.
[32] J. Zhang, X. Xu, L. Chen, An ultrasensitive electrochemical bisphenol A sensor based on hierarchical Ce-metal-organic framework modified with cetyltrimethylammonium bromide, Sens. Actuators B Chem. 261 (2018) 425–433.
[33] E. Laviron, Adsorption, autoinhibition and autocatalysis in polarography and in linear potential sweep voltammetry, Chem. Interfacial Electrochem. 52 (1974) 355–393.
[34] H.S. Yin, Y.L. Zhou, S.Y. Ai, Preparation and characteristic of cobalt phthalocyanine modified carbon paste electrode for bisphenol A detection, J. Electroanal. Chem. 626 (2009) 80–88.
[35] Q. Li, H. Li, G.F. Du, Z.H. Xu, Electrochemical detection of bisphenol A mediated by $[Ru(bpy)_3]^{2+}$on an ITO electrode, J. Hazard Mater. 180 (2010) 703–709.
[36] C. Yu, L. Gou, X. Zhou, N. Bao, H. Gu, Chitosan–Fe_3O_4 nanocomposite based electrochemical sensors for the determination of bisphenol A, Electrochim. Acta 56 (2011) 9056–9063.
[37] L. Yang, H. Zhao, S.M. Fan, B.C. Li, C.P. Li, A highly sensitive electrochemical sensor for simultaneous determination of hydroquinone and bisphenol A based on the ultrafine Pd nanoparticle@TiO_2 functionalized SiC, Anal. Chim. Acta 852 (2014) 28–36.
[38] F. Tan, L. Cong, X. Li, Q. Zhao, H. Zhao, X. Quan, J. Chen, An electrochemical sensor based on molecularly imprinted polypyrrole/graphene quantum dots composite for detection of bisphenol A in water sample, Sens. Actuators B Chem. 233 (2016) 599–606.
[39] F. Wang, J. Yang, K. Wu, Mesoporous silica-based electrochemical sensor for sensitive determination of environmental hormone bisphenol A, Anal. Chim. Acta 638 (2009) 23–28.
[40] L.A. Goulart, F.C.D. Moraes, L.H. Mascaro, Influence of the different carbon nanotubes on the development of electrochemical sensors for bisphenol A, Mater. Sci. Eng. C 58 (2016) 768–773.
[41] Y. Yang, H. Zhang, C. Huang, N. Jia, MWCNTs-PEI composites-based electrochemical sensor for sensitive detection of bisphenol A, Sens. Actuators B Chem. 235 (2016) 408–413.
[42] T.D. Vu, P.K. Duy, H.T. Bui, S.H. Han, H. Chung, Reduced graphene oxide–Nickel sulfide (NiS) composited on mechanical pencil lead as a versatile and cost-effective sensor for electrochemical measurements of bisphenol A and mercury (II), Sens. Actuators B Chem. 281 (2019) 320–325.
[43] K. Shim, J. Kim, M. Shahabuddin, Y. Yamauchi, M.S.A. Hossain, J.H. Kim, Efficient wide range electrochemical bisphenol-A sensor by self-supported dendritic platinum nanoparticles on screen-printed carbon electrode, Sens. Actuators B Chem. 255 (2018) 2800–2808.
[44] F. Mo, J. Xie, T. Wu, M. Liu, Y. Zhang, S. Yao, A sensitive electrochemical sensor for bisphenol A on the basis of the AuPd incorporated carboxylic multi-walled carbon nanotubes, Food Chem. 292 (2019) 253–259.
[45] H.S. Yin, Y.l. Zhou, S.Y. Ai, Preparation and characteristic of cobalt phthalocyanine modified carbon paste electrode for bisphenol A detection, J. Electroanal. Chem. 626 (2009) 80–88.